BACK-SCATTERED ELECTRON IMAGING OF A LATERITIC IRON ORE AND ITS APPLICATIONS IN PROCESS MINERALOGY

A. Alcover Neto and Reiner Neumann
Centro de Tenologia Mineral - CETEM
Rua 4, Quadra D
Rio de Janeiro - RJ - 21941-590 Brazil

C. L.Schneider
University of Utah
1460 East 135 South Room 412
Salt Lake City - UT - 84112-0114 USA

Abstract

A hydrocyclone treating an itabirite iron ore was sampled, characterized in detail using modern image analysis techniques and modeled. Some of the most interesting results from this investigation were:

1. The Itabirite studied is highly porous; this property may be advantageous in direct reduction applications.
2. Two types of porosity are present; one is macroscopic and the other microscopic.
3. The micro-pores in this itabirite are interconnected.
4. Porosity liberation in the size range studied is associated to the macro pores.
5. The process of liberation in this itabirite is quick, probably aided by liberation by detachment.
6. The regimen inside the hydrocyclone is closer to turbulent than it is to laminar regimen.
7. The density of the slurry in the separation zone must be used instead of the density of the liquid.

It is anticipated that lateritic iron ores in general may present significant porosity, and this must be taken into consideration when evaluating image analysis results from this type of ores.

Keywords: Liberation, Hydrocyclone, Image Analysis, Modeling.

Introduction

The work reported here originated from a need to implement quantitative image analysis for mineralogical characterization at CETEM's process mineralogy laboratory. CETEM is a fully equipped center for minerals technologies with services ranging from small scale lab tests to full pilot scale testing of most unit operations in mineral processing. Services and testing are supported by a complete chemical analysis laboratory, and a process mineralogy laboratory that includes modern X-Ray diffraction and an excellent Leica S-440 SEM equipped with X-Ray micro-analysis and a solid-state back-scattered electron detector. A research project in tandem with the University of Utah Center for Minerals Technology and SAMARCO, a major iron ore producing company in Brazil was carried out at CETEM. The aim was to execute a project that would cover most areas related to liberation characterization and process mineralogy, inducing the implementation of the techniques developed at the University of Utah at CETEM's mineralogy laboratory. The work consisted of a sampling campaign around a hydrocyclone operating in closed circuit with a ball mill at SAMARCO's Germano plant.

Samples were collected in the feed, overflow and underflow of the cyclone cluster, and all pertinent operation data recorded. The dry samples were screened using standard sieving, and delivered to CETEM for analysis. The work that ensued was that of sampling, mounting, grinding and polishing, carbon coating and image acquisition, all using standard techniques. The LEICA S-440 SEM is capable of unattended image acquisition and this is a crucial advantage since for proper statistics, about 50 images must be acquired from each narrow size sample, and for the 30 samples, 10 from each stream, this translates to 1,500 images to be acquired. Although unattended operation capability is largely due to stage configuration, capability of running 3 samples at a time in the chamber and a good stage control interface, it is also very important to maintain beam stability during the hours while the system is operating automatically. Combined with an even coating of carbon on the surface of the mounts, beam stability is perhaps the strongest feature of this SEM. Once the contrast and brightness are set according to the requirements for proper phase discrimination and the automated image processing procedures that followed, the peaks corresponding to the epoxy mounting media, quartz, goethite and hematite and magnetite, the main mineral components of this ore, are found at or near the preset grey levels in all images, without need for detector gain adjustments or any other kind of intervention during the acquisition process.

The LEICA system has a number of features designed for qualitative analysis. One of them is the visual display of the images at high contrast, even when actual contrast is poor. This feature must to be turned off for quantitative analysis, so that the images generated are true high-contrast images. This also helps in adjusting the solid state detector to the proper level of gain. Also, the image histogram can be displayed with the image, facilitating the adjustment of contrast and brightness.

Once a good image acquisition procedure was in place, implementation of the MMIA™ software package developed at the University of Utah was required. MMIA™ is developed under Solaris™, which is not available at CETEM. The low cost solution was to port MMIA™ to Linux. The workstations controlling the LEICA system, running a DOS based OS, and the Linux workstation were networked to CETEM's LAN, and communication could be established using standard TCP/IP over Ethernet. This is the basis for interfacing the image acquisition system with the MMIA™ image analysis system. With the implementation of a GUI for file exchange and management, implementation of MMIA™ at CETEM was completed.

Following the required implementation, the proposed work included training in image processing techniques, measurement of linear and areal liberation, stereological correction, process mineralogy calculations, and modeling and simulation of the cyclone with the liberation information obtained at CETEM. This was expected to be a straight forward repetition of work routinely done at the University of Utah. However, due to the lateritic characteristics of the Itabirite iron ore, the high porosity associated to the iron bearing minerals must be characterized before any useful result can be obtained. This is usually not necessary for the non-lateritic ores such as Taconite, lending novelty to the Itabirite characterization. Furthermore, liberation had never been fully characterized for any of the Brazilian Itabirites, even though liberation plays an important role in obtaining the high-grade concentrates that are required for pelletization. Finally, modeling the hydrocyclone with measured liberation spectra had never been reported in the literature,

and this exercise uncovered some long debated aspects of hydrocyclone operation in the light of the traditional Plitt (1976) model.

Itabirite Image Analysis

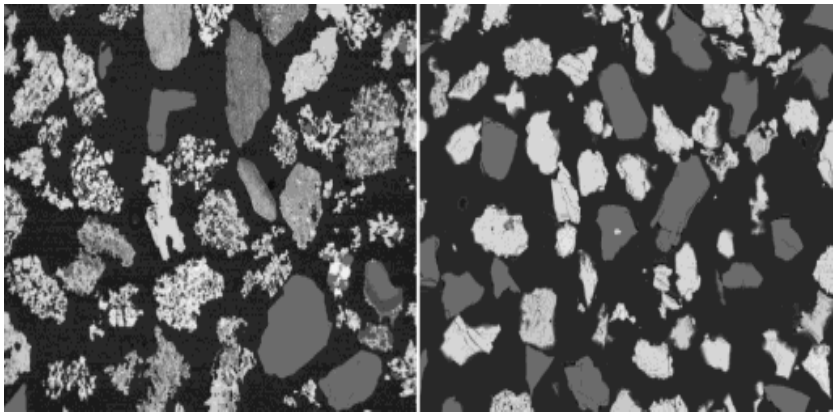

Figure 1:Cyclone overflow particles. Left image from 841x589 micron particles at 20X magnification. Right image from 44x37 micron particle at 600X magnification.

The Itabirite studied is mainly composed of quartz, goethite, hematite and magnetite. The average atomic numbers of hematite and magnetite are too close to allow for discriminating these two phases at the contrast levels used in this work. Goethite, quartz and the epoxy mounting media can be discriminated from hematite and magnetite so that whenever all phases are present in significant amounts, 4 peaks could be clearly identified in the grey level histogram of the solid-state backscatter electron image. The epoxy peak was located at about grey level 30 by adjusting the brightness level and then contrast was adjusted so that the peak corresponding to hematite/magnetite was located at grey level 220.

At first inspection, the images show particle cross-sections with significant amounts of porosity. Direct measurement in porous sections is not feasible, and the best course of action is to fill the features prior to measurement, using apparent densities to reconcile grades and volumetric grades after measurement. The quartz in the Itabirite has very little observable internal porosity, and it was assumed that all porosity is associated to the iron bearing minerals, with advantage, since pores located at the interface between quartz and an iron phase cannot be correctly identified as belonging to one phase or another. On the other hand, pores located completely inside quartz features were filled with quartz phase. Linear grade and areal grade distributions were measured on ternary images with a phase corresponding to the epoxy mounting media, one corresponding to gangue, mostly quartz and another that included goethite, hematite and magnetite, thus giving liberation of iron bearing minerals against the gangue minerals. Because grades must be reconciled, the amount of porosity associated

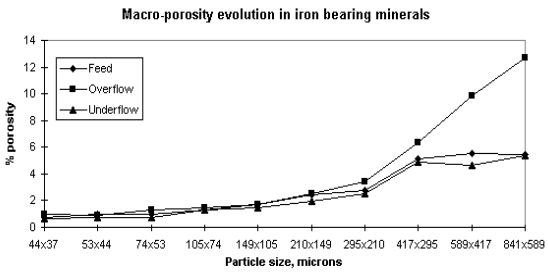

Figure 2: Measured porosity in each sample analyzed.

to the iron bearing minerals was recorded and saved for each image in each specimen. Furthermore, the volume fractions of goethite were measured in each image. This is important because goethite's density is considerably less than that of hematite, and because goethite and hematite are abundant phases in the itabirite, mass fractions calculated from volume fractions may be strongly influenced by the relative amounts of goethite and hematite. The mass fraction of any particular phase in a mineral system can be calculated when the volume fractions and densities of all phases present are known. When the volume fractions measured include the volume of the pores associated, then apparent densities must be used instead of phase densities. In any case, porosity must be known before mass fractions can be calculated. Other measurements carried out included feature and phase perimeters, chord length distributions and feature area distribution.

Qualitative and quantitative assessment of porosity by image analysis

The problem of quantitative analysis of the itabirite is better understood when one surveys every back-scattered electron image generated on all samples originating from each stream and size range. As an attempt to illustrate the essence of this process, two images from samples of hydrocyclone overflow are shown side by side in Figure 1, one from large particles at low magnification and one from small particles at high magnification. Significant amounts of porosity can be readily seen in the large particles and comparatively less porosity is seen in the small particles. Also, the general shape of the particles in both images is significantly different, with the large particles showing concavities in the perimeter of the cross-sections indicating that the fracture surface intercepts the unbroken ore pores frequently, while in the small particles the shape is significantly more convex, indicating that the process of pore liberation is not as significant at this size. This process has impact in the hydrocyclone operation, as particles with higher porosity tend to concentrate in the overflow stream while the less porous particles tend to concentrate in the underflow stream. The evolution of measured porosity with stream and size shown in Figure 2 confirms this tendency.

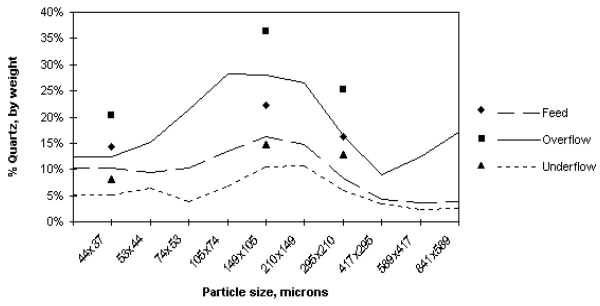

Figure 3: Quartz assays from chemical (symbols) and I.A. (lines) calculated using the measured macro-porosity.

Reconciliation of chemical and image analysis grades

Chemical assay of iron ore is performed routinely in a number of laboratories in Brazil. Nine samples, three from each stream, were selected and sent to two certified laboratories for detailed chemical analysis, and the mass fractions of quartz, goethite, hematite and magnetite determined. The assays from both labs were in agreement. The estimated mass fractions of quartz from image analysis, using the

measured porosity in each sample, are shown in Figure 3, and this is compared with the results of the chemical assays. Clearly the mass fractions of quartz were consistently underestimated in all samples, and this ultimately lead to the conclusion that the measured porosity by image analysis was consistently underestimated in all samples. The nature of the porosity of this itabirite began to be understood when particle density measurement was undertaken using a helium pycnometer. The measured densities were equal to the theoretical densities of the phases, given the contributions of each phase as calculated using chemical assay results. In clear terms, all the pores that are present in the particles and that can be clearly seen under the microscope, were filled with helium during the pycnometer measurement. The inexorable conclusion is that all pores must be connected to each other and to the particle surface, since the helium flows freely through the pores. Interestingly enough, the same problem in reconciling I.A. results with chemical assays have been reported by Fandrich (1998) who measured liberation in a lateritic iron oxide sample probably originated in South Africa, and reported a significant degree of porosity not visible to QEM*SEM used in that work, and in the work reported by Srivastava et al (1999) who studied the Kiriburu lateritic iron ore of India. Also corroborating the presence of micro-porosity, is the amenability of some itabirites to direct reduction precesses. Sampaio et al (1997) showed that the kinetics of direct reduction of a Brazilian itabirite was considerably faster when using H_2 when compared to CO as reduction gas in a fluidized bed reactor, and attributed this to the presence of inter-crystalline micro-pores.

Because magnetite cannot be distinguished from hematite in back-scattered electron images, it was assumed that magnetite and hematite constituted a single phase. This assumption can be considered mild in this case since only small amounts of magnetite is present, less than 5% by weight. Also, it was assumed that the same amount of porosity is present in the goethite phase and the hematite/magnetite phase, which may be unrealistic, but does not prevent porosity to be evaluated in a general basis. With these assumptions, porosity can be calculated using

$$P = 1 - \frac{\rho_{Qz} V_{Qz}}{\rho_G \bar{V}_G + \rho_{HM} \bar{V}_{HM}} \left[\frac{1}{M_{Qz}} - 1 \right] \qquad (1)$$

where ρ_{Qz}, ρ_G *and* ρ_{HM} are the densities of quartz 2.65 g/cm^3, goethite 4.26 g/cm^3 and hematite/magnetite 5.2 g/cm^3 respectively, V_{Qz}, $\bar{V}_G$ *and* $\bar{V}_{HM}$ are the measured volume fractions of quartz, goethite and hematite/magnetite by image analysis. The bars indicate when the measured volume includes porosity. M_{Qz} is the mass fraction of quartz from chemical assay and P is the total porosity (micro- and macro-porosity combined).

Table I: Calculated micro-porosity from chemical and image analysis assays in hydrocyclone feed samples

		Chemical Assay			Calculated Porosity		Image Analysis		
	Size, µm	M_{Qz} %	M_G %	M_{HM} %	P_{macro} %	P_{micro} %	V_{Qz} %	$\bar{V}_G$ %	$\bar{V}_{HM}$ %
Feed	44x53	14.30	18.64	67.06	0.99	36.36	16.28	24.11	59.61
	105x149	21.86	26.60	51.54	1.69	29.62	26.29	22.04	51.67
	210x297	15.60	34.67	49.73	2.78	48.63	14.23	27.92	57.85

Results for the feed stream are shown in Table I, and the absolute values of porosity calculated are huge, with micro-porosities ranging from 30% to 50%. This may be the very reason why direct reduction in mini- mills is becoming so popular in Brazil during the past few years.

Liberation measurement results

Liberation of itabirite is comparatively easy, with most particles completely liberated at about 300 µm. Unliberated particles with sizes larger than 300 µm are mostly particles with high iron bearing minerals content, in the 90-100% volumetric grade range. Particles of size larger than 600 µm are almost completely unliberated. The complete process of liberation takes place on the 600 to 300 µm size range. It is believed that porosity contributes to this quick liberation process, since most macro-pores observed were in the quartz-hematite, quartz-goethite interfaces, probably and likely causing the quartz grains to liberate by detachment, which is a mode of liberation that is never observed in non-lateritic ores. Surely, this property is most advantageous to the itabirite iron industry. The overall liberation spectra for all sizes, after stereological correction, and conversion to weight fractions, in the three hydrocyclone streams is shown in Figure 4, and is represented by the symbols in the figure.

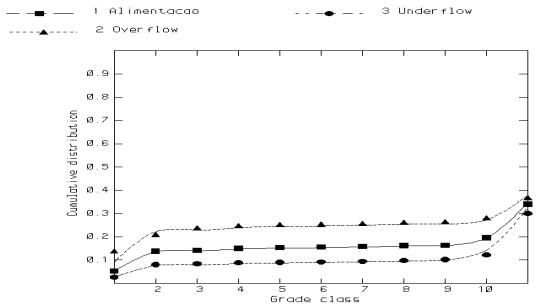

Figure 4: Measured (symbols) and calculated (lines) liberation spectra around the hydrocyclone.

Hydrocyclone modeling with liberation data

The separation of the feed into a high grade and a low grade product is clearly shown in Figure 4, and this is due to strong concentration effects with respect to particle density in the hydrocyclone. Plitt's model (Plitt , 1976, and Flintoff et al, 1987) for the hydrocyclone is used here as implemented in MODSIM™ to simulate this operation. The underlying idea in Plitt's model is to estimate the cut size, sharpness of separation and short circuit to underflow based on the hydrocyclone geometry and the operational conditions. The required variables for Germano's hydrocyclone are listed in Table 2. MODSIM™ is *liberation ready* and the liberation spectra per size can

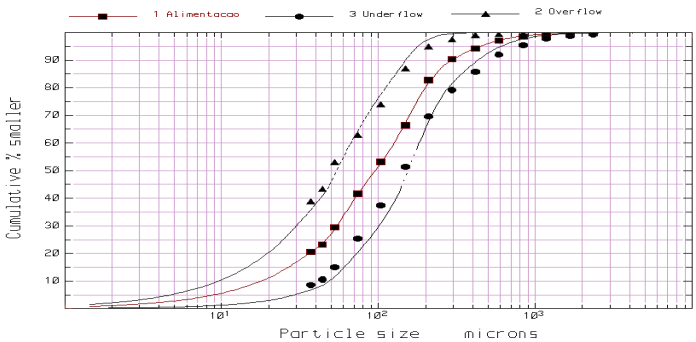

Figure 5: Measured (symbols) and calculated (lines) size distributions in the three sampled hydrocyclone streams.

be entered as system data, besides flowrates, solids contents and particle size distributions. The original Plitt model, as published in 1976, embeds particle density in the calculation of the cut size d_{50}. This is shown in equation (2).

$$d_{50} = \frac{50.5\ D_c^{0.46}\ D_i^{0.6}\ D_o^{1.21}\ e^{(0.063\ \varphi)}}{D_u^{0.71}\ h^{0.38}\ Q^{0.45}(\rho_s - \rho)^{0.5}} \qquad (2)$$

In equation 2, Q is the volume flowrate of slurry in the hydrocyclone feed, ρ_s is the particle density and ρ is the density of the liquid (water). All other parameters are specified in Table II (see Plitt, 1976 for the appropriate units). In equation 2, d_{50} varies with particle density, and the result is that a different value of d_{50} must be calculated for each particle composition, or particle type. In this work, all iron bearing minerals were considered as a single phase, with average density of 3.5 g/cm^3, which is very low when compared to that of pure hematite, but is a good estimate of bulk density based on the high values of porosity encountered in the ore characterization section. The density of pure gangue particles was taken as the density of quartz, 2.65 g/cm^3. Ten additional particle types are defined according to the measured liberation spectra, and each of these particle types have a density between 2.65 g/cm^3 and 3.5 g/cm^3 as defined by their composition. The problem of applying Plitt's model with liberation information is therefor straight forward, and each particle type will have a characteristic d_{50}, as calculated in equation 2.

Table II: Characteristics of the sampled hydrocyclone cluster.

Hydrocyclone diameter, Dc	0.6604 meters
Vortex finder diameter, Do	0.2032 meters
Inlet diameter, Di	0.2540 meters
Apex diameter, Du	0.1143 meters
Vortex finder - spigot distance	3.96 meters
Solids in the feed slurry, φ	58.65 %
Solids feed rate	1640 TPH
Pressure drop across cyclone, H	10 meters of H_2O
Number of cyclones in cluster	6

The model provides three additional correction factors, one for the cut size, one for the sharpness of separation and one for the short-circuit to underflow. These parameters are calculated from the experimental data, under the operational conditions that are required, using an optimization procedure. Normally, only particle size distributions in the three streams are available to estimate the correction factors. In this work, measured grade distributions must also be predicted by the model, simultaneous with the measured size distributions. The three size distributions measured are represented by the symbols in Figure 5. When calculating the correction factors, which is essentially the only modeling work that is required to simulate the hydrocyclone, a lack-of-fit is observed in both predicted size distributions and predicted grade distributions, and the lack-of-fit was particularly high in the predicted grade distributions. The model, as implemented, was clearly not capable of describing the hydrocyclone operation. However, one should

revisit Plitt's original work before drawing any precipitated conclusion. To quote Plitt, page 121 in his original 1976 publication,

"One factor which was not specifically investigated in this work was the solid-liquid density difference. The relationship assumed in equation (2) was that for laminar settling:

$$d_{50} \propto (\rho_s - \rho)^{-0.5}$$

This relationship had been nearly universally accepted until Lynch (1975), recently determined that the exponent in the relationship may be closer to the turbulent settling value of -1. With d_{50} sizes ranging up to several hundred microns, it is conceivable that the flow relative to the particle may be the turbulent rather than laminar. With high-density pulps, it is also possible that it would be more reasonable to use the slurry density rather than the liquid density in this relationship. This is an area which perhaps deserves further study, particularly in relation to slurries which contain minerals of different densities."

Well, this is just the case here, so a decision was made to re-implement the optimization procedure to calculate also the regiment exponent and the slurry density in equation (2), besides the three correction factors, to fit simultaneously the size and grade distributions measured. The resulting fit is excellent, and this is represented by the continuous lines in Figures 4 and 5. The parameters for this fit are: correction factor for d_{50} = 4.9067, sharpness = 0.38833 and solids bypass = 0.70023, and d_{50} is proportional to:

$$d_{50} \propto (\rho_s - 2.26)^{-0.90}$$

showing that the regimen inside the hydrocyclone is much closer to turbulent than it is to laminar and that the slurry density in the hydrocyclone separation zone should be used instead of the density of the liquid.

References

Fandrich, R.G., 1998. *Mineral Liberation Through Confined Bed Breakage*, Ph.D. Thesis, University of Queensland.

Srivastava, M.P., Pan, S.K., Prasad, N., 1999. "Characterization and Processing of Iron Ore Fines of Kiriburu Deposit of India," submitted to the *International Journal of Mineral Processing*

Sampaio, R.S., Souza Neto, A.N., Fujikawa, L.H., Garcia, L.R.A., Pereira, R.O.S. and Reis, J.A.S., 1997. "Avaliação de minério de ferro para processos de redução direta em leito fluidizado," Anais do 2º Congresso Internacional de Tecnologia Metalúrgica e de Materiais, São Paulo.

Plitt, L.R., 1976. "A Mathematical Model of the Hydrocyclone Classifiers," *CIMM Bull.*, Vol 69, No. 776, pp. 114-123.

Flintoff, B.C., Plitt, L.R. & Turak, A.A., 1987. "Cyclone modeling: a review of present technology, *CIMM Bull.*, Vol. 80, No. 905, pp. 39-50.

Lynch, A.J. & Rao, T., 1975. "Modeling and Scale Up of Hydrocyclone Classifiers,", Proc. 11th Intl. Min. Proc. Cong., Cagliari.